International Conference on Ships and Offshore Structures
ICSOS 2017
11 – 13 September 2017, Shenzhen, China

Vortex Induced Vibration of Long Flexible String with Moderate Mass Ratio in Uniform Current

Chong Sun[a], Dixia Fan[b1], Wanhai Xu[a], Chuning Ji[a], Michael S. Triantafyllou[b]

[a] *Tianjin University, 135 Yaguan Road,Tianjin, 300350, China*
[b] *Massachusetts Institute of Technology, 77 Mass Ave, Cambrdige MA-02136, USA*

Abstract

Laboratory tests have been performed on a long flexible string with an aspect ratio of 240 (length to diameter) and a moderate mass ratio of 4.0 (structural mass to displaced fluid mass) undergoing vortex induced vibration. The model was vertically installed, resulting in a linearly varied tension spanwise and was towed to generated uniform flow with different speeds, achieving Reynolds number from 250 to 3000. Optical measurement with an array of high speed cameras was applied and managed to accurately obtain both temporally and spatially dense information on the cross-flow (CF) and in-line (IL) vibration. It was observed in the current experiment high modal vibration up to 7th in the CF direction and 14th in the IL direction. The high modal response displayed "multi-modal" vibration which contained a mixture of standing and traveling wave pattern, resulting in an asymmetrical distribution of displacement without clear nodes. Meanwhile the non-dimensional frequency (vibration frequency to modal natural frequency) and phase between CF and IL have been studied and they showed a strong connection related to the CF and IL modal group.

Keywords: VIV; Flexible cylinder; Modal switch;

1. Introduction

Risers play key roles in the deep-water oil industry, as they are lifelines between the wellhead and the floating platform, transferring oil and gas from the seabed to the water surface. One of the top design challenges for the riser system is the accumulating fatigue issue since it is constantly exposed to oscillatory vortex induced loads [14] and therefore undergoes non-stopping vibration. A large amount of research efforts has been dedicated to the fundamental understanding of the vortex induced vibration (VIV) of rigid cylinders [2, 6, 15] and their connection to the VIV of flexible cylinders [11] which are closer representations for offshore riser modeling. However, the question still remains whether the current rigid cylinders VIV model is accurate enough or even valid to be the building blocks to predict flexible cylinders VIV [1].

Previous work by Huera-Huarte [7-8] experimentally investigated flexible cylinders vibrating at the 1st mode in the CF direction. The results revealed that for low tension cases, flexible cylinders responded similar to 1-degree-of-freedom (CF) elastically mounted rigid cylinders with three branches (initial, upper, lower) of response vs. reduced velocity. At the same time, the lower response branch will disappear with the increase of the tension. However, in the similar work by Mu [13] with 1st CF mode excited, the lower brunch response persists for all the tension cases.

* Corresponding author. Tel.: +1-857-259-8454; fax: +1-617-253-8125.
E-mail address: dfan@mit.edu

Furthermore, one of the major differences between the elastically mounted rigid cylinders and flexible cylinders is that, instead of single natural frequency, flexible cylinders acquire infinite number of natural frequencies and their corresponding natural modes. And hence, compared to rigid cylinders VIV for narrow reduced velocity range, flexible cylinders are potentially excited over a much wider range of reduced velocity [1]. And the problems will become even more complicated, as for the nowadays deep-water drilling riser, their aspect ratio (length to diameter) can reach over 10^3 and even to10^4 and this will result in the total riser response of a tension-dominated, high modal vibration pattern with potential presence of multi-modal contribution and traveling wave [12].

In this paper, it presents the experimental work performed in the MIT tow tank on the vortex induced vibration of a vertically installed, tension dominated flexible string with an aspect ratio of 240 and mass ratio of 4.0. Model was dragged with different speed, achieving Reynolds number from 250 to 3,000 and reduced velocity from 4.8 to 40. It was observed in the current experiment single frequency and narrowband vibration dominating in each case and it was achieved high modal vibration up to 7^{th} in the CF direction and 14^{th} in the IL direction, based on results of the modal analysis. It shows a strong connection between the string modal shapes, non-dimensional frequency and phase between CF and IL across the span. In addition, compared to standing wave, single-modal CF response for the low reduced velocities, the string dominates by traveling wave pattern, resulting in an asymmetrical distribution of displacement without clear nodes for the high reduced velocities. The purpose of current work is to help us a better understanding of the detailed physics of VIV of the flexible cylinders, as well as to serve as a benchmark for future CFD model comparison (with moderate Reynolds number of 250 to 3000 that current CFD codes may handle.).

2. Experimental Model and Method Description

2.1 Experimental Arrangement

The experiments were carried out at MIT tow tank facility. The experiment towing length was 30.48 m and, in all the tests, the water depth was kept in 1.22 m. An aluminum frame was built to provide stiff mounting points for the model. The tests were carried out by driving the carriage in always the same direction along the tank.

The model was vertically installed and towed to generate uniform flow with different speeds from 0.05 to 0.6 m/s, achieving Reynolds number from 250 to 3000 and reduced velocity from 4.8 to 40 (The reduced velocity is linked to the natural frequency which is calculated based on the mean tension in each experimental run.). The cylinder dimensions were d = 0.5cm in diameter, L = 120cm in length, giving an aspect ratio of 240 (length to diameter) and 4.0 in mass ratio (structural mass to displaced fluid mass). And in the current experiment, the immersed length to total length was 95%. The model used the silicon rubber material and the damping ratio of this model is 8.7%.

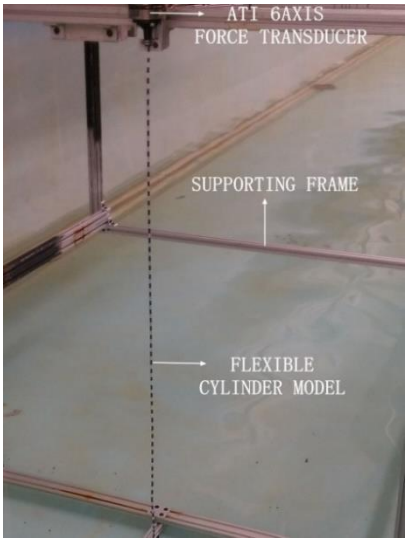

Fig. 1. Experimental setup with flexible cylinder (total length 120cm, diameter 0.5cm)

A 6-axis load cell was installed at the top to measure the top tension of the riser during the experiments. Total 52 points (staggered black and white markers) along the model were tracked by the underwater optical measurement system with an array of high speed cameras [3] which were installed both beside and behind of the model for simultaneous IL and CF vibration measurement. A sketch of camera and model arrangement and a sample of the measured image are shown in Fig. 2. Compared to the traditional strain-gauge and accelerometer measurement for flexible cylinder VIV experiment, optical tracking system provides both temporally and spatially dense measurement, which helps to reveal more physical phenomena missed by older measurement tools [4].

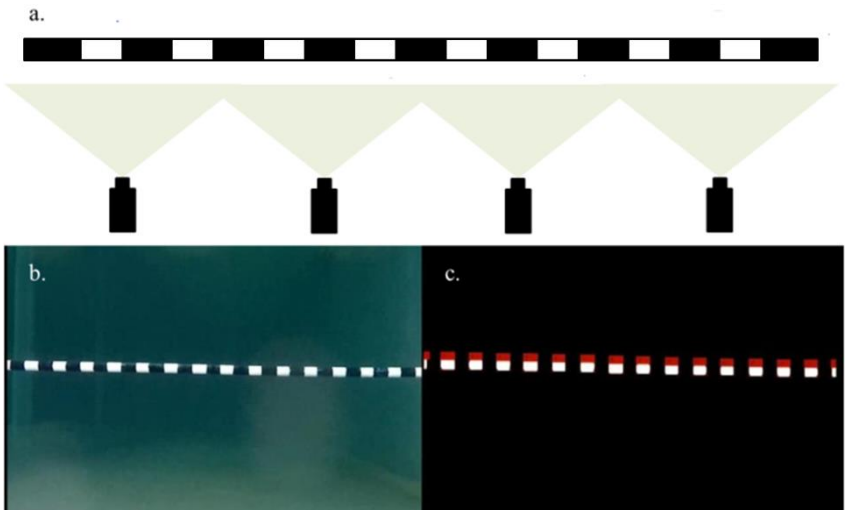

Fig. 2. Camera arrangement and a sample case: a. Sketch of 4 cameras coverage of the riser model in the CF direction, overlapping of each camera images will be used in the spatial synchronization; b. Sample image from one camera for the CF measurement; c. Processed image of Fig.2 b with image processing and motion tracking algorithm (the red bounding box shows the ability to capture and follow the motion of the white markers)

2.2 Analysis Methodology

2.2.1 Modal approach

In the current study, modal decomposition analysis [9] was used to help identifying the standing wave mode number being excited for the flexible string due to the vortex shedding, and its procedure is described as following. The IL and CF deflections of the riser from its static condition are denoted by $x(z,t)$ and $y(z,t)$. Boundary conditions are provided by the zero displacements at both ends. And hence the displacements in IL and CF directions can be expressed in terms of time-dependent modal weights u and v .

$$x(z,t)-\bar{x}(z)=\sum_{n=1}^{N}u_n(t)\varphi_n(z),\ z\in[0,L] \tag{2.1}$$

$$y(z,t)=\sum_{n=1}^{N}v_n(t)\varphi_n(z),\ z\in[0,L] \tag{2.2}$$

Where t is the time, z the vertical coordinate, L the length of the riser, $\bar{x}$ the time-averaged IL displacement, $\varphi_n(z)$ the mode-shape, $n=1,2.3,\ldots,N$, $u_n(t)$ and $v_n(t)$ the modal weight of IL and CF directions, $n=1,2.3,\ldots,N$. It is assumed that N terms are enough to describe displacement in the current experiment.

In the current study, restoring forces due to tension are much larger compared with restoring forces due to bending stiffness, hence the bending stiffness can be negligible. The normalized mode-shapes of a string under linearly changed tension [10] can be expressed as:

$$\psi_n = \frac{Y_0(y_b)J_0(y) - Y_0(y)J_0(y_b)}{J_0(y_b)} \tag{2.3}$$

Where Y_0 and J_0 are, respectively, the first and second Bessel function of zero order, and

$$y = \frac{2\sqrt{mT_z}}{\omega}\omega_n \tag{2.4}$$

Where m is the mass per unit length, T_z the axial tension of point z, ω the unit weight of riser, and ω_n the natural frequency of the n-mode. And T_z can be expressed as

$$T_z = T_b + \omega z = T_b + (T_t - T_b)\frac{z}{l} \tag{2.5}$$

T_b and T_z are, respectively, the bottom tension and top tension of the riser. ω_n can be obtained by solving equation (2.6):

$$Y_0(y_t)J_0(y_b) - Y_0(y_b)J_0(y_t) = 0 \tag{2.6}$$

Where $y_b = \frac{2\sqrt{mT_b}}{\omega}\omega_n$, $y_t = \frac{2\sqrt{mT_t}}{\omega}\omega_n$.

The mode-shapes of the riser can be obtained after normalization processing,

$$\varphi_n = \frac{Y_0(y_b)J_0(y) - Y_0(y)J_0(y_b)}{J_0(y_b)} \cdot \frac{1}{\max(\psi_n(z))} \tag{2.7}$$

The CF direction is modally decomposed as described in the following. Displacement is measured at a number of positions on the riser, z_m, $m = 1, 2, ..., M$;

$$c_m(t) = y(t, z_m),\ m = 1, 2, ..., M \tag{2.8}$$

Here $c_m(t)$ is the measurement signal after filtering the measurement noise.

It is assumed that the mode-shapes $\varphi_n(z)$ are known and N terms are sufficient to describe the displacement,

$$c_m(t) = \sum_{n=1}^{N} v_n(t)\varphi_n(z_m),\ m = 1, 2, ..., M \tag{2.9}$$

This equation can be expressed in vector notation. First, form the vector of mode-shape displacement of measured points:

$$\boldsymbol{\varphi_n} = [\varphi_1(z_1), \varphi_n(z_2), ..., \varphi_n(z_M)]^T, n = 1, 2, ..., N \tag{2.10}$$

Then form the $M \times N$ vector:

$$\boldsymbol{\phi} = [\boldsymbol{\varphi_1}, \boldsymbol{\varphi_2}, ..., \boldsymbol{\varphi_N}] \tag{2.11}$$

Then form the vector of displacement and time-dependent modal weights:

$$\boldsymbol{c(t)} = [c_1(t), c_2(t), ..., c_M(t)]^T \tag{2.12}$$

$$\boldsymbol{v}(\boldsymbol{t}) = [\omega_{\boldsymbol{1}}(t), \omega_{\boldsymbol{2}}(t), ..., \omega_N(t)]^T \tag{2.13}$$

Eq. (2.9) can now be written as

$$\boldsymbol{c}(\boldsymbol{t}) = \boldsymbol{\phi v}(t) \tag{2.14}$$

And the modal weights can be expressed as

$$\hat{\boldsymbol{v}}(\boldsymbol{t}) = (\boldsymbol{\phi}^T\boldsymbol{\phi})^{-1}\boldsymbol{\phi}^T\boldsymbol{c}(\boldsymbol{t}) = \boldsymbol{H}\boldsymbol{c}(\boldsymbol{t}) \tag{2.15}$$

the modal decomposition of the IL direction is as same as the CF direction.

2.2.2 Phase analysis

The phase between CF and IL vibration at each location is one of the key characters of the VIV, as it is strongly associated with the energy transfer between the fluid and structure. For the steady vibration, IL vibrates normally as twice fast as in the CF direction, and hence the phase between them cannot be simply obtained via Fourier analysis and callas for the Hilbert Transform [5], as following.

Let $w(t)$ be a signal and $\boldsymbol{H}(w)$ its Hilbert Transform. The Hilbert Transform allows representing the instantaneous phase $\theta_w(t)$ and amplitude $A_w(t)$ of signal, in the form:

$$\boldsymbol{H}(w) = A_w(t)e^{i\theta_w(t)} \tag{2.16}$$

The phase-shift between two signals is then given by

$${}^{m}_{n}\theta^{q}_{p}(t) = -\beta\theta^{p}_{n}(t) + \theta^{q}_{m}(t) \tag{2.17}$$

Where *n* and *m* refer to the mode number, *p* and *q* represent the direction (IL or CF) and β is the ratio between the dominant frequency of the two signals.

3. Experimental Results

3.1 Statistics

In the current experiment, statistically, both standard deviations and 1/10 highest peaks are used to describe the IL *x* and CF *y* vibration magnitude over model length *z*.

The form of the standard deviations is defined as

$$\sigma_x = \sqrt{\frac{1}{T}\int_0^T \frac{1}{L}\int_0^L [x(z,t) - \bar{x}(z)]^2 dzdt} \tag{3.1}$$

$$\sigma_y = \sqrt{\frac{1}{T}\int_0^T \frac{1}{L}\int_0^L y^2(z,t) dzdt} \tag{3.2}$$

Where $\bar{x}(z)$ is the time-averaged IL displacement.

In the Fig. 3(a), the time average top tensions are plotted against the reduced velocity $U_r = U/f_1 d$, in which f_1 is the fundamental natural frequency of the model the in the still water (assuming the added mass coefficient to be 1.0 along the model). With the increase of the reduced velocity U_r, the drag force along the model increases and it has to be balanced with the horizontal component of the tensions, resulting in the quadratic rise of the tension. The tension change will affect the modal natural frequency,

and it has been taken into account the calculation of the reduced velocity. In the Fig. 3(b), it was plotted the maximum time average inline model displacement $\bar{x}_{max}/d$ against reduced velocity. As the mean drag force is proportional to the reduced velocity square, the $\bar{x}_{max}/d$ displays the similar quadratic increase trend with the best fit of $\bar{x}_{max}/d = C(U/f_1 d)^2$, with $C = 0.0072$ in the current study. At the same time, we can also see there are cases when the $\bar{x}_{max}/d$ departs from the fitted data, suggesting a variation of the mean drag coefficient.

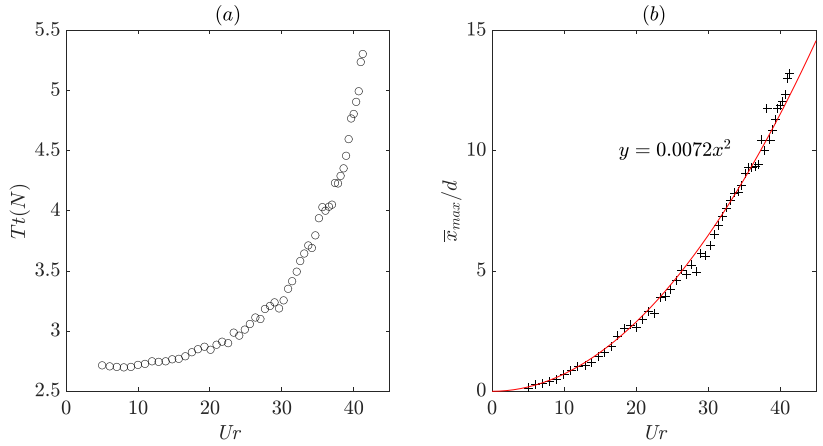

Fig. 3. (a) Time averaged top tension and (b) maximum time averaged inline displacement against the reduced velocity *Ur*. (Solid line in the (b) is the best quadratic fit of the data)

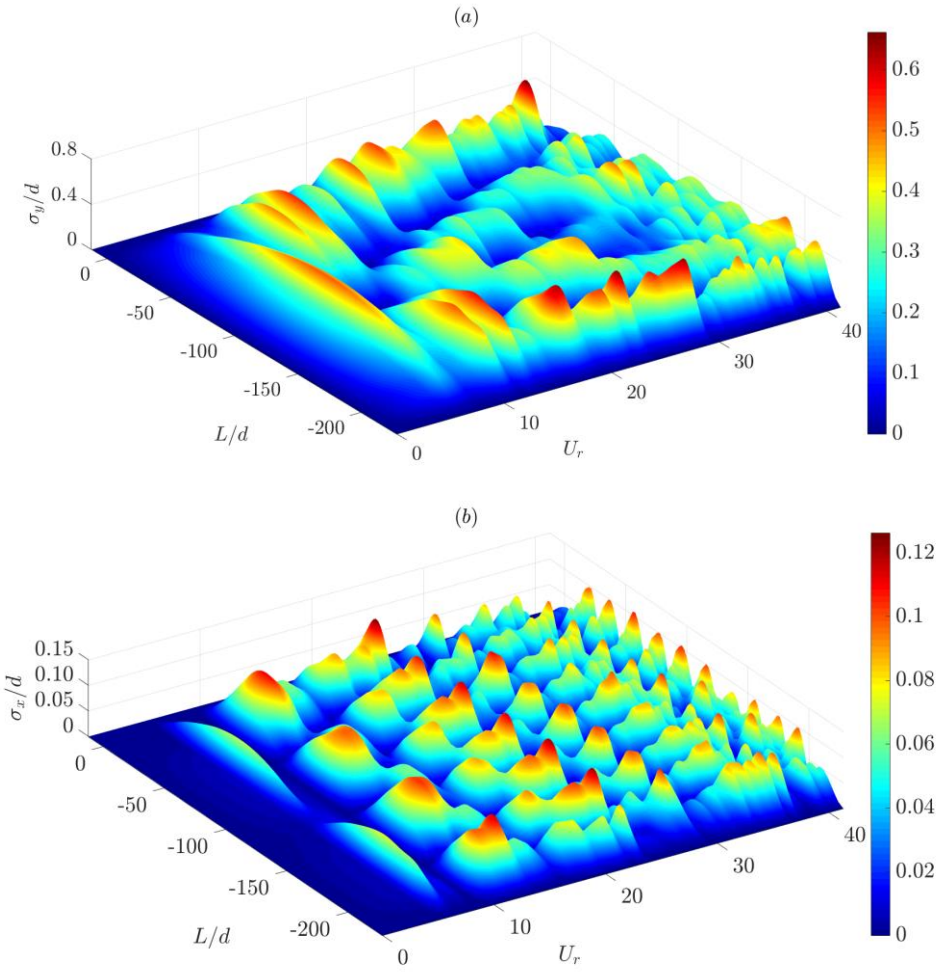

Fig. 4. Standard deviations of CF (a) and IL (b) displacement along the model span against the reduced velocity.

Fig. 4(a) and 4(b) presents the standard deviations of the cross flow and IL displacements in the plan of length against the reduced velocity. The results show that with the increase of the reduced velocity, the vibrational pattern of the model changes with clear increase of the excited mode number in both CF and IL direction. And in the current experiment, the maximum 7th CF mode and 14th IL mode have been excited.

In the Fig. 5(a) and 5(b), three cases of different reduce velocity at 9.99, 25.53 and 35.16 are picked out for standard deviation of the CF and IL displacement. We can see that at lower reduced velocity, CF displacement is responded in a standing wave pattern with a clear identification of both nodes (where CF displacement closes to zero) and peaks. But at higher reduced velocity, CF response is rather "flat" and no clear node can be easily identified, which means a standing wave pattern of CF response can't be observed. However, in the IL direction, over all the reduced velocity range in the current experiment, model displayed a standing wave pattern with nodes that can be clearly identified.

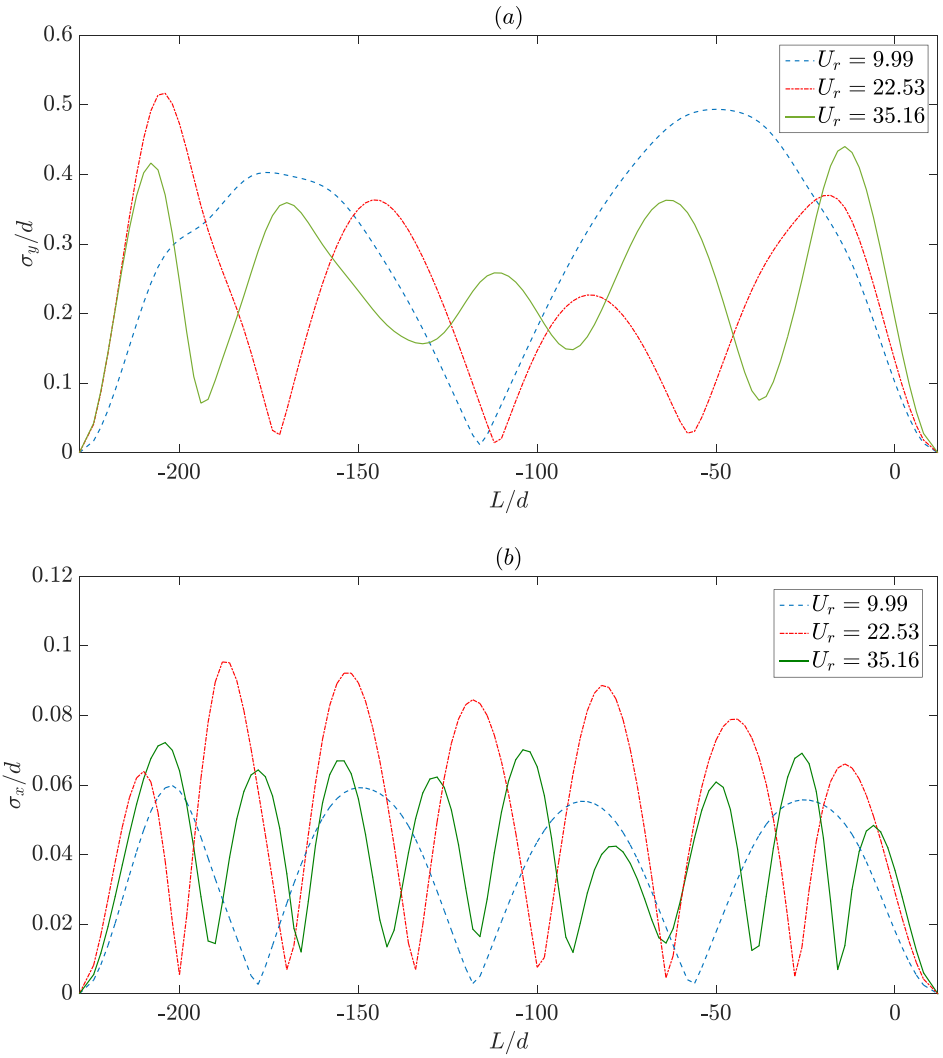

Fig. 5. Standard deviations of CF (a) and IL (b) displacement along the model span for three reduced velocity.

3.2 Modal Analysis

Modal analysis first performs on the CF response, and the modal weight against reduced velocity is plotted in the Fig. 6. It shows the modal number increase in steps with the increase of the reduced velocity. And for the reduced velocity smaller than 30, the modal response is mainly dominated by single mode, while for the cases of higher reduced velocity, the results display a much wider spread modal weight distribution.

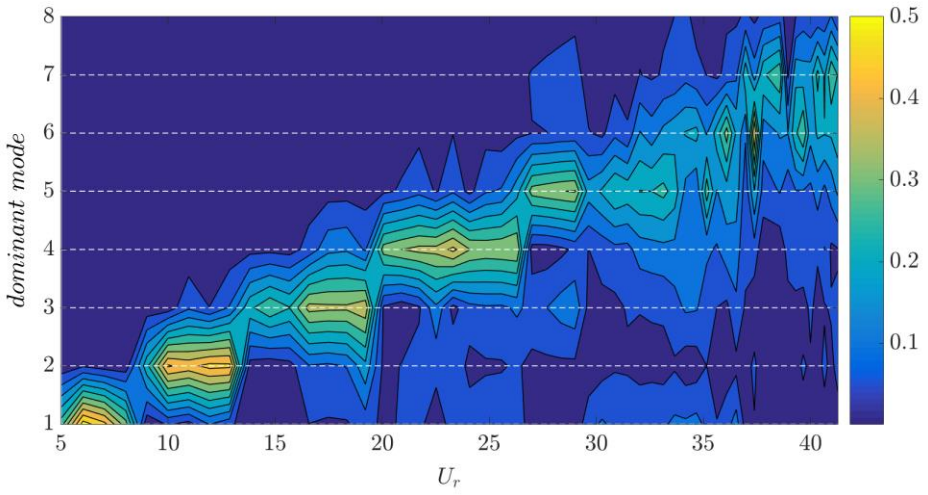

Fig. 6. Modal weight of the CF response vs. reduced velocity

In order to reveal this difference between single modal weight dominated vibration and multiple modal weights contributed vibration, time series of displacement and separated modal weight for two reduced velocity at 14.76 and 33.66 are picked out along the model and plotted in the Figs. 7-10.

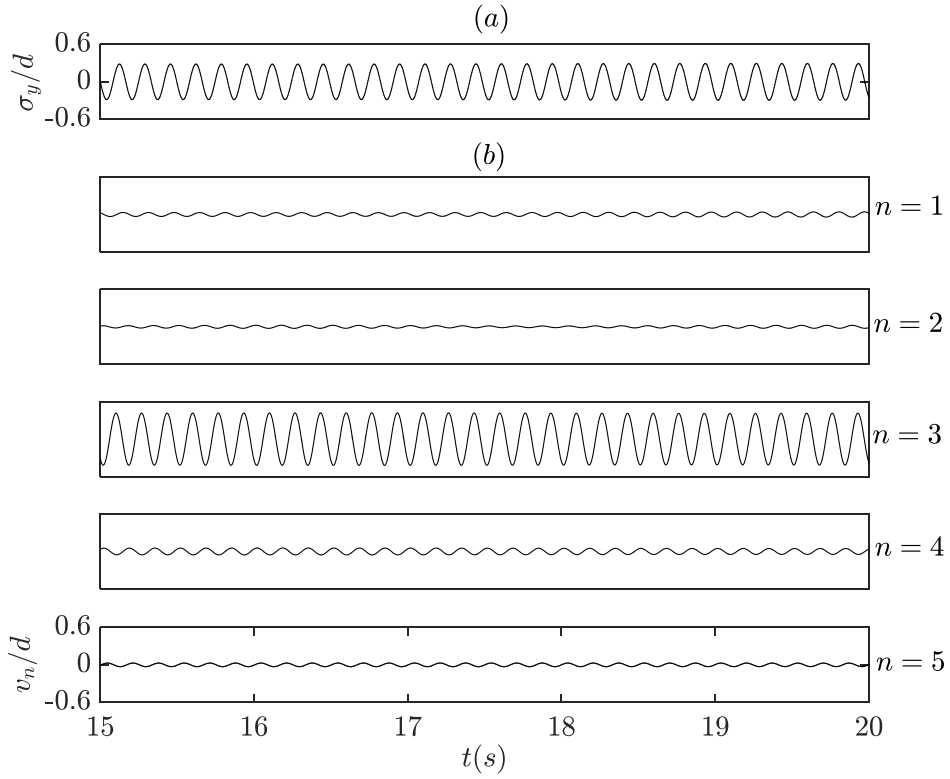

Fig. 7. (a) Time series of CF displacement for *Ur* = 14.76 at L/d = -96. (b) Time series of separated modal weight (1-5).

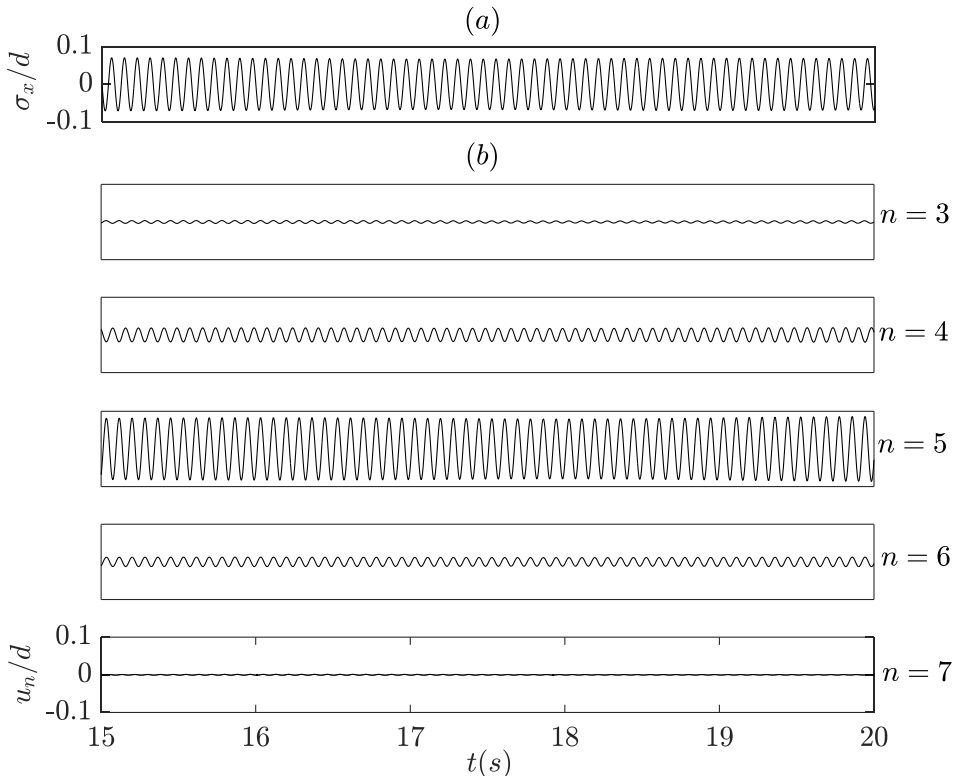

Fig. 8. (a) Time series of IL displacement for *Ur* = 14.76 at L/d = -96. (b) Time series of separated modal weight (3-7).

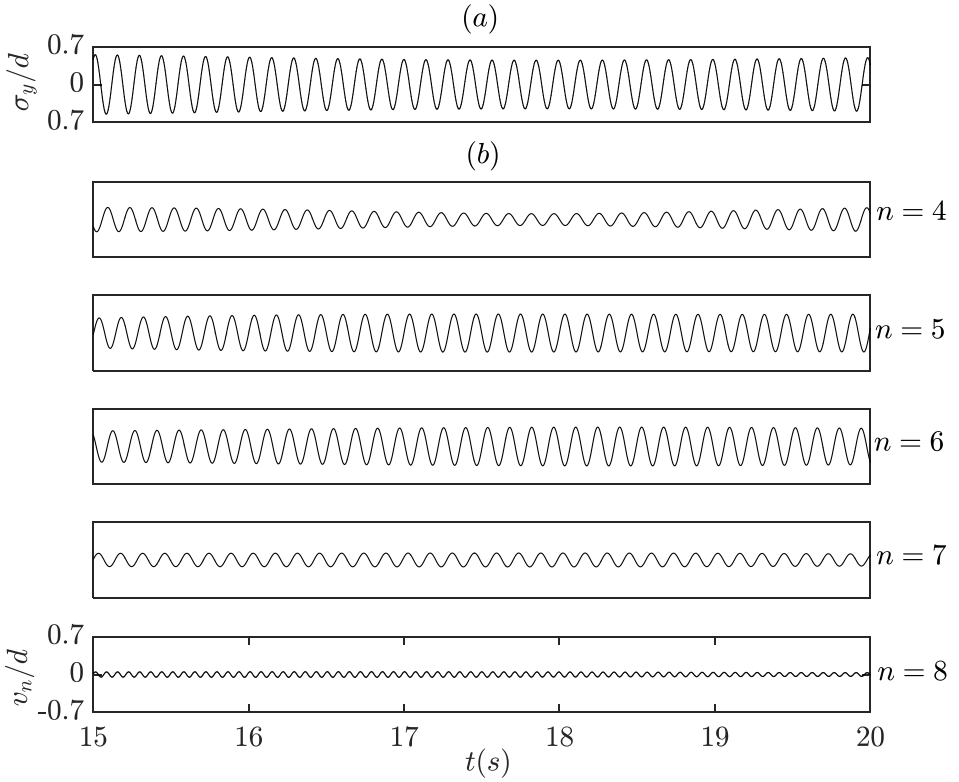

Fig. 9. (a) Time series of CF displacement for *Ur* = 33.66 at L/d = -96. (b) Time series of separated modal weight (4-8).

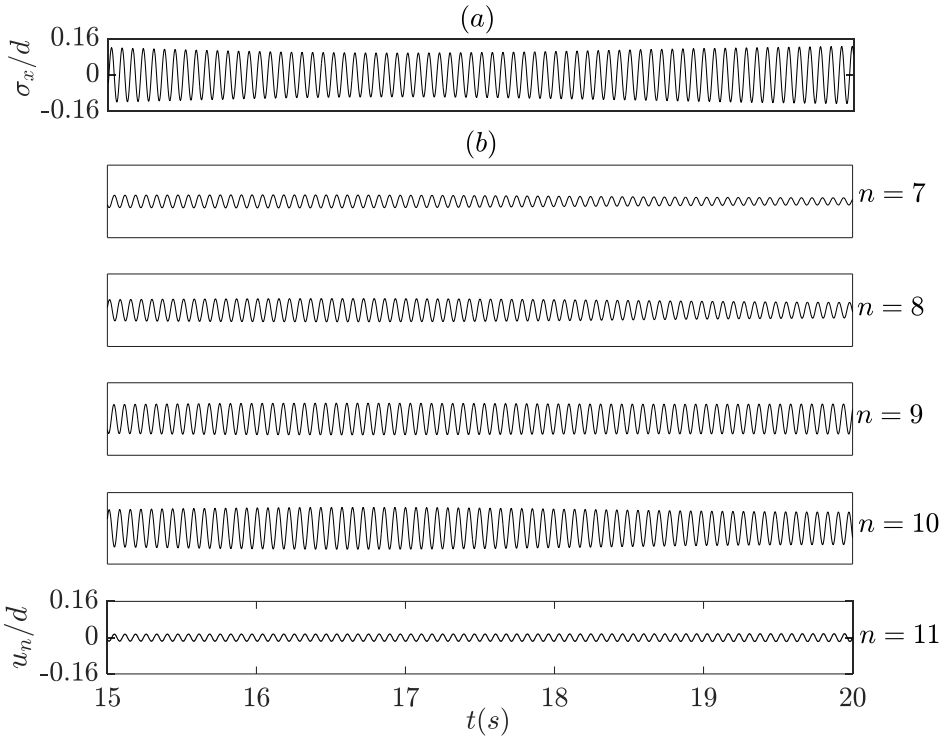

Fig. 10. (a) Time series of IL displacement for *Ur* = 33.66 at L/d = -96. (b) Time series of separated modal weight (7-11).

In the Figs. 7 and 8, it shows that at reduced velocity of 14.76, the vibration has one strong dominant mode of 3th (CF) and 5th (IL) that overpowers all the neighboring modal weight, hence a single modal weight vibration. On the contrary, for the case of reduced velocity of 33.66, it is of comparable strength for 5th and 6th modal weights in the CF direction and 9th and 10th modal weights in the IL direction. And it is important to note that such multiple modes coexist at the same time, instead of sharing different time period, which cannot be explained by the modal switch.

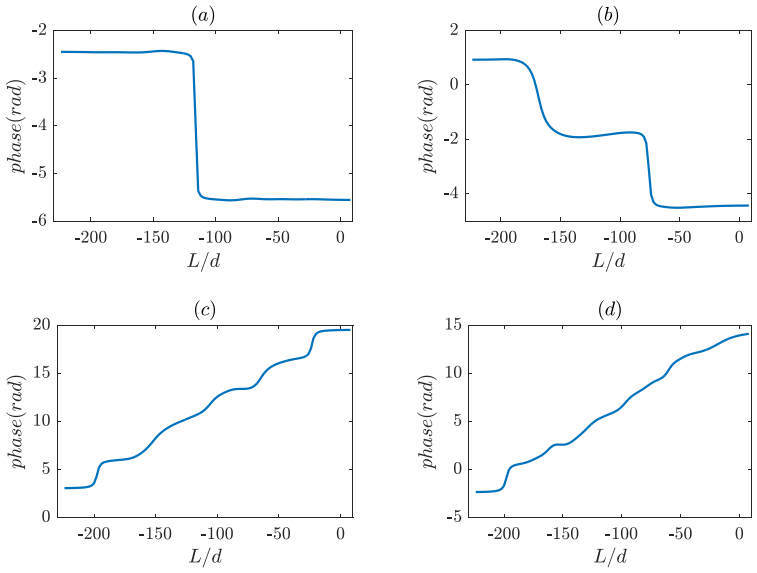

Fig. 11. Spatial phase distribution for (a) Ur = 9.99. (b) Ur = 19.22. (c) Ur = 39.66. (d) Ur = 41.28.

Spatial phase along the model is then calculated for the CF response via Fourier analysis and plotted in the Fig. 11 for 4 different reduced velocities, together with the standard deviation of the CF response across the model. The result shows that at the lower reduced velocity, spatial phase jumps at the node and keeps a constant value between the nodes. This result indicates that model in the current experiment at low reduced velocity, CF responds in a standing wave pattern. However, for the higher reduced velocity cases of Ur = 39.66 and Ur = 41.28, it can be identified that the phase drifts in one direction spatially in the CF direction across the majority part of the model and jumps at the boundary, while the standard deviation of the CF response is rather "flat" with no clear nodes. It indicates that for higher reduced velocity cases, model displays a traveling wave dominant response with a mixture of standing wave. And for such traveling wave dominant response, modal displayed an asymmetrical response with maximum CF displacement found close to the boundary. And this is due to the reflection of the traveling wave from the end, which altogether superpose into a local standing wave pattern close to the boundary. And as a matter of fact, in the current experiment, the identified multiple modal vibration pattern is actually caused by the traveling wave response without clear nodes that cannot be captured by the current modal analysis, assuming a standing wave pattern.

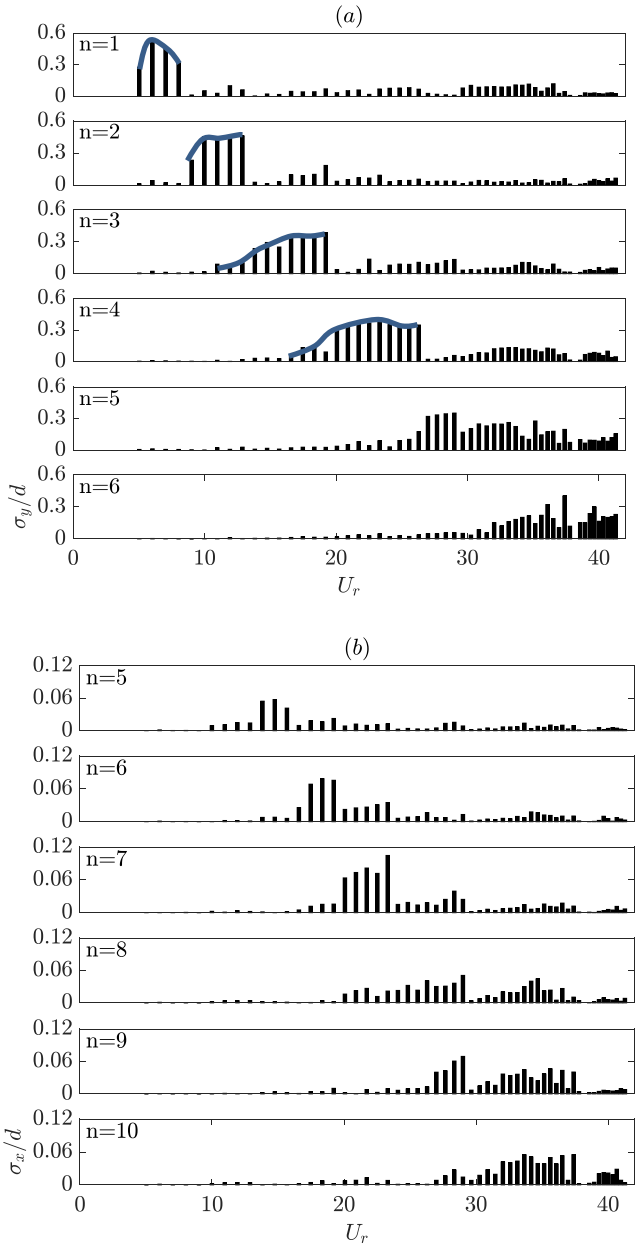

Fig. 12. Measurements of standard deviations of (a) IL and (b) CF amplitude of oscillation as function of reduced velocity.

Standard deviations of separated modal weights that are significant to vibration response in the current experiments are plotted in the Fig. 12. (Fig. 12(a) includes 1st ~6th modes of CF response and Fig. 12(b) includes 5th ~10th modes of IL response). Each modal weight occupy certain range of the reduced velocity with a slowing growing trend in amplitude but drop drastically when next mode catches up. In addition, both "initial excitation branch" and "lower branch" of amplitude response can be seen in 1st mode, but only "initial excitation branch" can be observed in modes higher than 2nd in cross-low response. Standard deviations of individual modes reach 0.12 diameters IL and 0.6 diameters CF.

3.3 Frequency Analysis

A typical result of the frequency analysis of CF and IL response for reduced velocity of 28.35 at different positions over the model is plotted in fig. 13. In the current experiments of uniform cylinder open to the uniform current, the model displays a narrow banded single frequency response along the whole model. In the fig. 13(b) of IL response, there are two frequency components. The dominating one corresponds to the twice of the CF vibrational frequency (second harmonic term) found in the Fig. 13(a) and the other is of the same frequency as the CF direction.

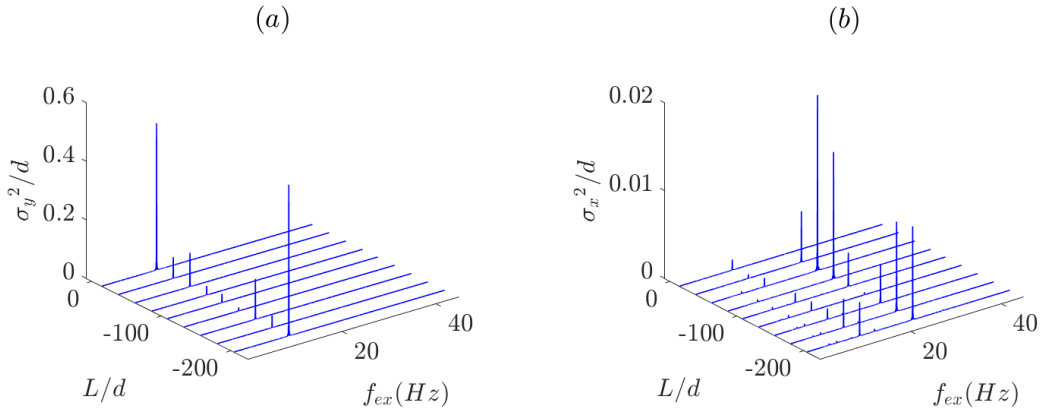

Fig.13 Dominant frequencies in (a) CF and (b) IL response when reduced velocity is 28.35.

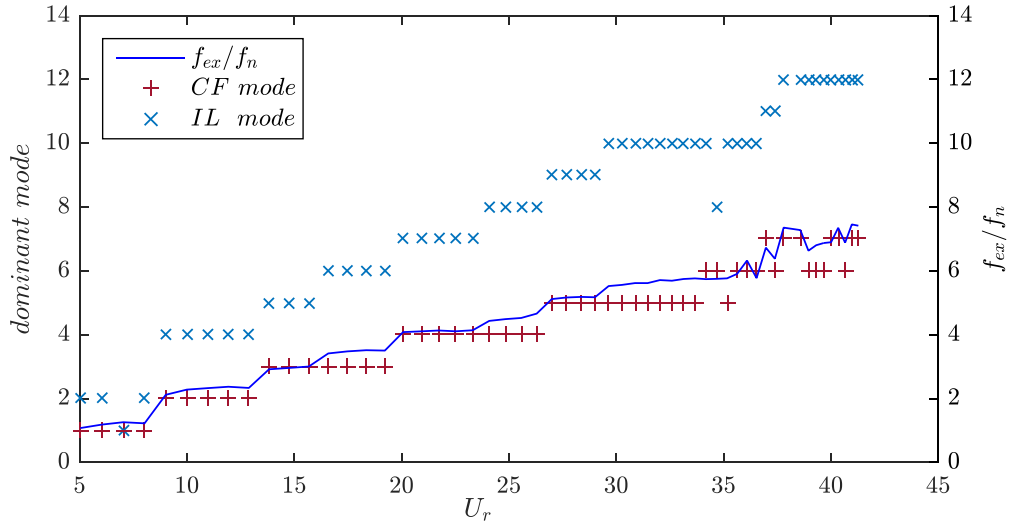

Fig.14 Measurements of CF response frequencies and dominant modes in IL and CF directions as functions of reduced velocity.

Normalized by the corresponding fundamental frequency f_1 in each test, the non-dimensional frequency f_{ex} / f_1 of CF and IL response are plotted against the reduced velocity in the Fig. 14, together with the dominated CF and IL mode number picked out from the modal analysis. The result shows that the f_{ex} / f_1, like the modal change pattern, increase in steps with the reduced velocity. As a matter of fact, such jump occurs when the dominant mode switches. In addition, Fig. 14 also reveals that while CF

and IL modes will jump at the same reduced frequency, IL mode makes more frequent jump than CF mode to catch the twice the mode number of the CF, and meanwhile, such IL mode jump also affects the f_{ex} / f_1 of the CF response (e.g. when reduced velocity increases from 23.31 to 24.08, the IL dominant mode change from 7th to 8th, while CF dominant mode keeps at 4th. And the CF frequency shows a little jump).

The maximum of the 1/10th highest peak of the CF and IL response are plotted against the reduced velocity in the Figs. 15 and 16 separately, and they are labeled in group with the dash line for same mode groups (the model responds in the same dominant CF and IL mode.). And the normalized frequency f_{ex} / f_1 is also plotted together.

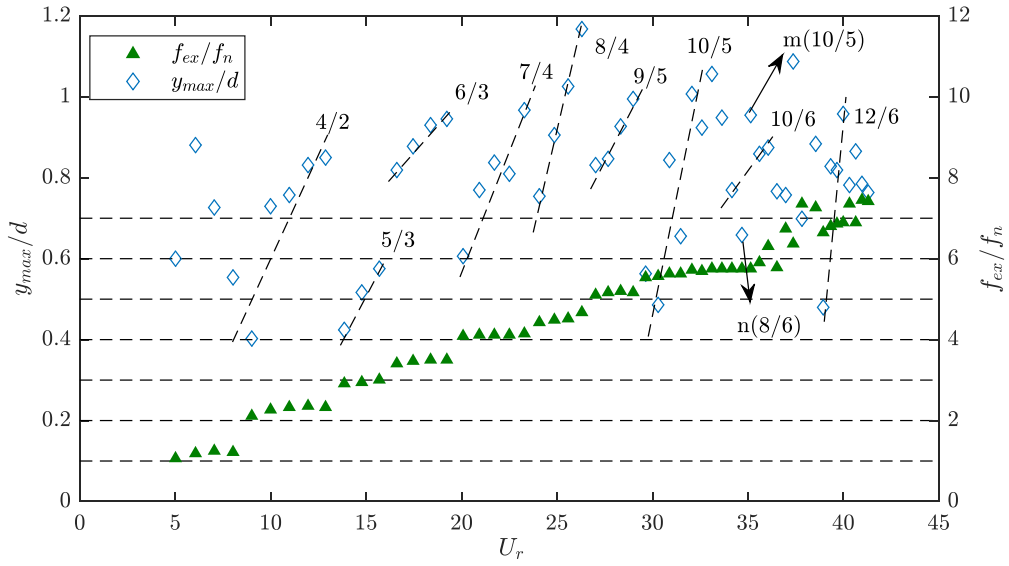

Fig. 15. Amplitude response of CF oscillation computed over time intervals and CF response frequency against reduced velocity, groups of points are identified by broken lines labeled with (dominant IL mode/ dominant CF mode) named “mode group”.

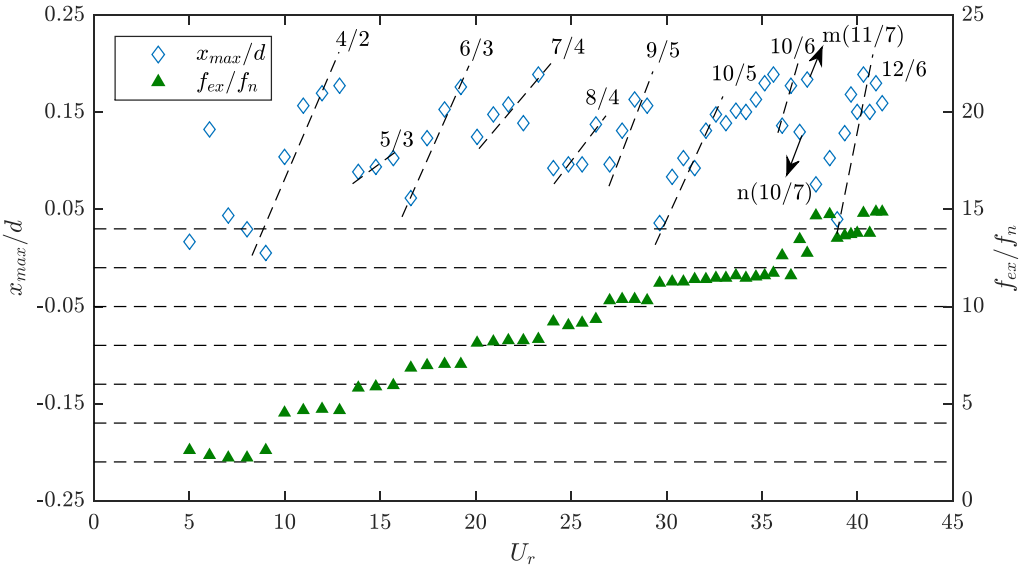

Fig. 16. Amplitude response of IL oscillation computed over time intervals and IL response frequency against reduced velocity

The result shows that the maximum amplitudes drop between two modal groups under conditions in which the modal weights show obvious moderation and dominant modes change, which can be seen in the case when reduced velocity changes from 12.88 to 13.82, the dominant CF modes are 2nd and 3rd (and

dominant IL modes 4th and 5th). Besides, it can be also observed that a jump in the dominant IL mode (without change in the dominant CF mode) can also lead to the jump of amplitude response in both directions, and the response frequency can be higher when the dominant IL mode is twice than the dominant CF mode than other cases, examples can be provided by the groups labeled 5/3 and 6/3, 7/4 and 8/4. The dominant IL mode will be higher but no more twice than dominant CF mode (the current experiment obtains two major modal group with IL and CF modal number ratio of 2:1 and 2(n-1):n.). It is also interesting to note that at high reduced velocity, the amplitude and frequency response become confusing and jump frequently against the reduced velocity. For points *m* and *n* plotted in Fig. 15, the amplitude shows huge difference at almost the same reduced velocity, which suggest that the change of modal content can lead to a huge impact of vibration response of flexible cylinder, which is sensitive to small changes of reduced velocity.

3.4 Phase Analysis

The phase angle between the CF and IL is one of the key factors for the VIV, as it determines the energy transfer direction whether from fluid to structure or reversely [2]. Phase between IL and CF vibration has therefore been analyzed. It is interesting to note a new phenomenon of phase time drifting that occurs at the onset of the 2:1 mode group. When the dominant IL mode jumps into twice than CF mode, dominant IL mode is changed without any change of dominant CF mode, phase between IL and CF is found drifting in time all along the entire model, as shown in the Fig. 17 (a-d) for the reduced velocity of 16.58 and 24.08 with the mode group of 3/6 and 4/8. And this results in a "messy" and irregular motion between IL and CF, which can be seen from the Fig. 19(a). However, shown in the Fig. 18(a-d) for the reduced velocity of 13.82 and 20.07, for the onset of the mode group of (2n-1): n, constant phase over time persists for the entire model length. And this will result in the persistently regular 8-figure motion between IL and CF in Fig. 19(b).

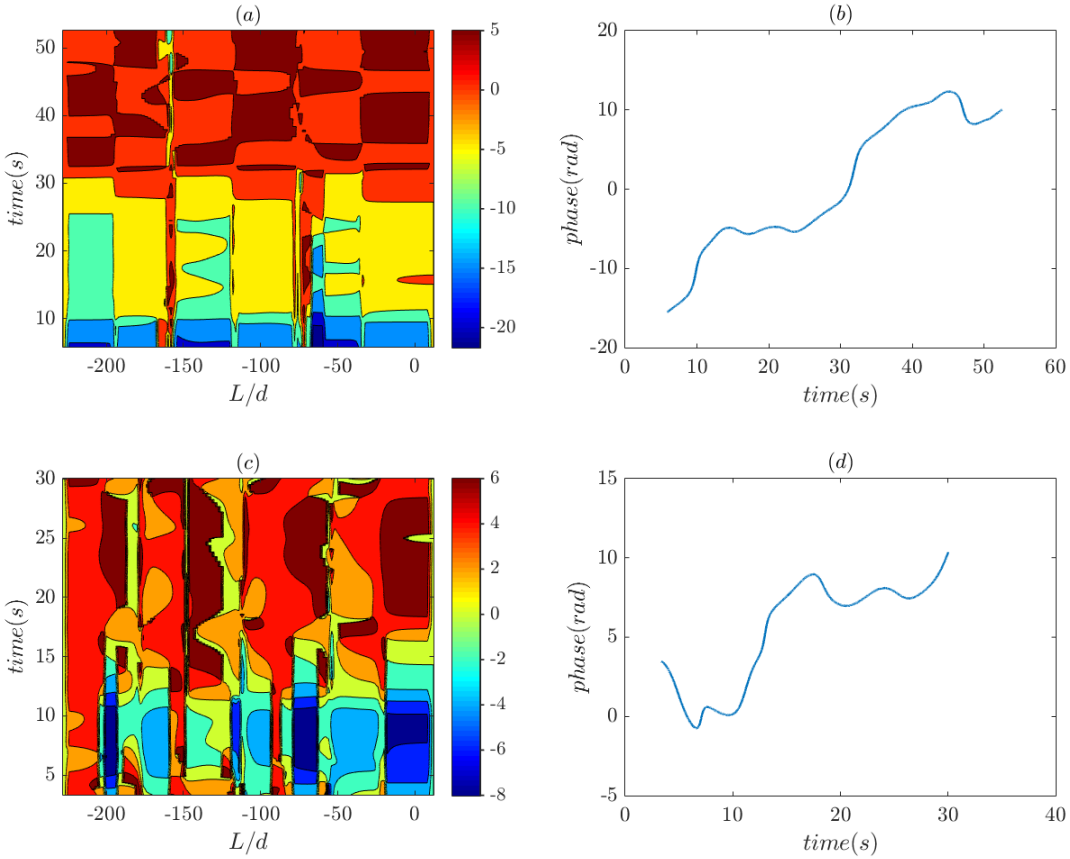

Fig. 17. Temporal and spatial phase distribution for (a) *Ur* = 16.58, (c) *Ur* = 24.08. Temporal phase distribution for (b) *Ur* = 16.58, (d) *Ur* = 24.08 at L/d = -128.

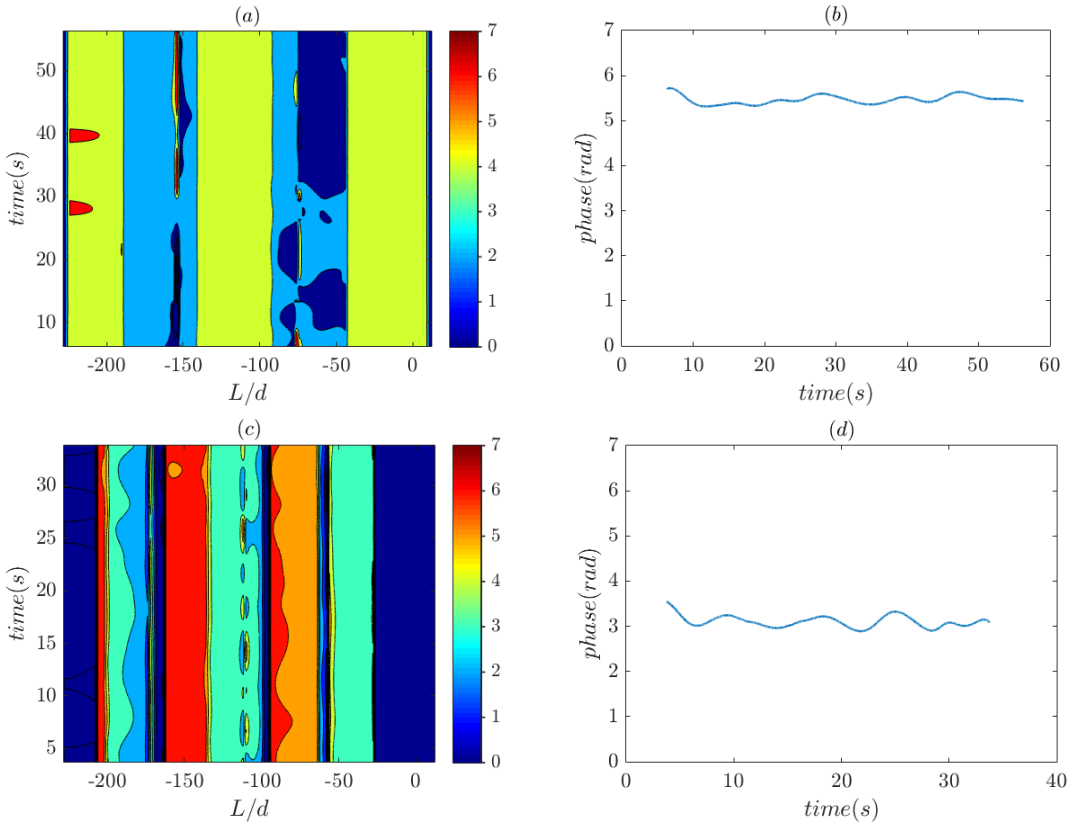

Fig. 18. Temporal and spatial phase distribution for (a) *Ur* = 13.82, (c) *Ur* = 20.07. Temporal phase distribution for (b) *Ur* = 13.82, (d) *Ur* = 20.07 at L/d = -128.

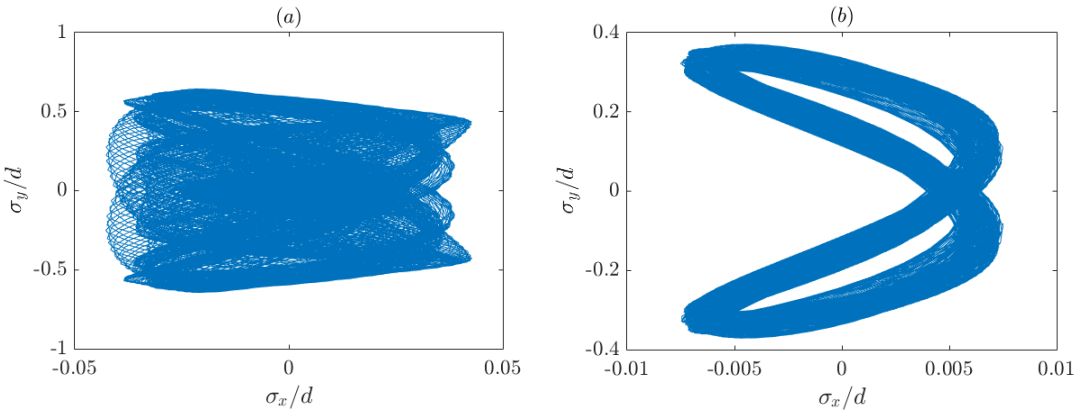

Fig. 19. Vibration motion between CF and IL for (a) *Ur* = 16.58, and (b) *Ur* = 13.82 at L/d = -128.

4. Conclusions

In the current research, experiments have been performed on the vortex induced vibration of a vertically installed, tension dominated flexible string with an aspect ratio of 240 and mass ratio of 4.0, and 95% submerged length. The test was performed under the uniform flow condition by dragging the model with different speed, achieving Reynolds number from 250 to 3,000 and reduced velocity from 4.8 to 40. Detailed dynamic IL and CF response of the model was captured by optical measurement technique with an array of high speed camera. Such technique has greatly benefitted our measurement and understanding of the problem, as, compared to traditional strain gauge and accelerometer measurement, it provides a robust non-intrusive measurement with both high spatial and temporal resolutions.

It is observed in the current experiment coherently narrowband single-frequency vibration dominating in each case. With the increase of the reduced, the dominant mode based on the modal analysis increases in steps for both IL and CF direction, and the current experiments achieves modal vibration up to 7th in the CF direction and 14th in the IL direction for the highest reduced velocity. For the low reduced velocity, the flexible string response display as a single modal, standing wave dominated response with nodes that can be clearly identified for both CF and IL direction. With the increase of the reduced velocity, the CF response becomes "flat", as no clear nodes to be observed. Spatial phase analysis shows that the string CF response is dominated by a mixture of the standing and traveling waves, resulting in an asymmetrical distribution of displacement without clear nodes. And this explains the result of multiple modes contribution from the modal analysis, assuming standing wave modes.

The experiment reveals that CF and IL dominant modes will jump at the same reduced frequency, and yet IL mode makes more frequent jump than CF mode to catch the twice the mode number of the CF. Meanwhile, at the jump of the dominant mode either in the CF or in the IL direction, it accompanies with the jump of the normalized dominant frequency. Based on IL to CF modal number ratio, there are two distinctive mode groups being identified in the experiments that is ratio of 2:1 and (2n-1): n. Result shows for IL to CF modal number ratio of 2:1, the vibrational frequency is larger than the modal frequency, indicating an averagely smaller added mass distribution along the model.

The modal switch over the reduced velocity strongly affects the maximum vibration amplitude over the flexible cylinder. The result shows that the amplitude will rise with the increase of the reduced velocity in the same modal group but commonly experience a sudden drop between the modal changes. Analysis on the phase between IL and CF vibration further reveals an interesting phenomenon that for the onset of the mode group of (2n-1): n, constant phase over time persists for the entire model length, while phase time drifting occurs at the start of the 2:1 mode group

References

1. Chaplin, J. R., Bearman, P. W., Huarte, F. H., & Pattenden, R. J. 2005. Laboratory measurements of vortex-induced vibrations of a vertical tension riser in a stepped current. *Journal of Fluids and Structures, 21(1)*, 3-24.
2. Dahl, J. J. M. 2008. Vortex-induced vibration of a circular cylinder with combined IL and CF motion. (*Doctoral dissertation, Massachusetts Institute of Technology*)
3. Fan, D., Du, H., & Triantafyllou, M. 2016, November. Optical Tracking Measurement on Vortex Induced Vibration of Flexible Riser with Short-Length Buoyance Module. In *APS Division of Fluid Dynamics Meeting Abstracts*.
4. Fan, D., and Triantafyllou, M. 2017. Vortex Induced Vibration of Riser with Low Span to Diameter Ratio Buoyancy Modules. The *Twenty-Seventh International Ocean and Polar Engineering Conference*. International Society of Offshore and Polar Engineers 2017.
5. Franzini, G. R., Pesce, C. P., Gonçalves, R. T., Fujarra, A. L., & Mendes, P. 2016. Experimental investigations on Vortex-Induced Vibrations with a long flexible cylinder. Part I: modal-amplitude analysis with a vertical configuration. In Proceedings of the *11th International Conference on Flow-Induced Vibration*, FIV 2016.
6. Gopalkrishnan, R. 1993. Vortex-induced forces on oscillating bluff cylinders. (*Doctoral dissertation, Massachusetts Institute of Technology*)
7. Huera-Huarte, F. J., & Bearman, P. W. 2009. Wake structures and vortex-induced vibrations of a long flexible cylinder—part 1: dynamic response. *Journal of Fluids and Structures*, 25(6), 969-990.
8. Huera-Huarte, F. J., & Bearman, P. W. 2009. Wake structures and vortex-induced vibrations of a long flexible cylinder—part 2: drag coefficients and vortex modes. *Journal of Fluids and Structures*, 25(6), 991-1006.
9. Lie, H., & Kaasen, K. E. 2006. Modal analysis of measurements from a large-scale VIV model test of a riser in linearly sheared flow. *Journal of fluids and structures*, 22(4), 557-575.

10. Rao, Z. B., Yang, J. M., Shi-Xiao, F. U., & Run-Pei, L. I. 2010. Prediction of vortex-induced vibration of a SCR under shear current. *Journal of Vibration & Shock*, 29(10), 4-8+98.
11. Triantafyllou, M., Triantafyllou, G., Tein, Y. S., & Ambrose, B. D. (1999, January). Pragmatic riser VIV analysis. In *Offshore technology conference*. Offshore Technology Conference 1999.
12. Vandiver, J. K., Jaiswal, V., & Jhingran, V. 2009. Insights on vortex-induced, traveling waves on long risers. *Journal of Fluids and Structures*, 25(4), 641-653.
13. Wu, H., Yan, S., Zhao, M., Lu, L., & Du, H. 2016, October. Laboratory Test on Dynamic Response of a Flexible Cylinder in Uniform Flow Using Optical Measurement. In *The Twelfth ISOPE Pacific/Asia Offshore Mechanics Symposium*. International Society of Offshore and Polar Engineers.
14. Xu, Y., Fu, S., Chen, Y., Zhong, Q., & Fan, D. 2013. Experimental investigation on vortex induced forces of oscillating cylinder at high Reynolds number. *Ocean Systems Engineering, 3(3),* 167-180.
15. Zheng, H. 2014. The influence of high harmonic force on fatigue life and its prediction via coupled inline-crossflow VIV modeling. (*Doctoral dissertation, Massachusetts Institute of Technology*)